Available online at www.sciencedirect.com

ScienceDirect

Physics Procedia 12 (2011) 56–65

Physics Procedia

LiM 2011

Effect of electromagnetic Stirring on the Element Distribution in Laser Beam Welding of Aluminium with Filler Wire

M. Gatzen*, Z. Tang, F. Vollertsen

BIAS - Bremer Institut für Angewandte Strahltechnik GmbH, Klagenfurter Straße 2, 28359 Bremen, Germany

Abstract

Additional external electromagnetic fields are used in laser beam welding of aluminium with silicon containing filler wire to manipulate the flow of the liquid metal due to induced volume forces and hence to modify the element distribution. Aiming for a better understanding of the fluid-dynamic processes inside the meld pool, a CFD model has been implemented to simulate the melt flow.

In this paper, simulation results on the resulting element distribution of filler wire material under a coaxial magnetic field with different frequencies is compared to experimental results for the same parameters. It is shown that in both cases the concentration of alloying elements of the filler material has a spatial periodicity. From the CFD model it can be concluded that the change of the distribution of the filler material results from a modulation of the melt flow due to the periodic induced electromagnetic volume forces.

Keywords: laser beam welding; magnetohydrodynamic; simulation; aluminium

1. Introduction

The use of magnetic fields is common in a variety of applications and well known in the metal industry, e.g. in continuous casting of steel, often used to achieve a refined grain structure [1]. Using steady and alternating magnetic fields in arc welding is also well understood, aiming predominantly at a stabilisation of the arc. Also, a distinct effect on the weld bead shape and dendrite growth was observed [2] due to a manipulation of the melt flow. The interaction between a conducting fluid and a magnetic field is treated in the magnetohydrodynamic theory [3]. Since nearly no liquid metal has a magnetic order, the interaction is based only on induction. That necessitates either a time dependent magnetic field or a fluid that is moving through the magnetic field.

In laser welding, the use of magnetic fields to influence the welding process has been investigated [4] and is also part of recent research activities [5]. It was shown that, by applying a steady magnetic field, the shape of the resulting seam cross section can be significantly influenced [6]. Using high frequency magnetic fields, a surface pressure can be induced that is capable of supporting the melt pool and thus avoiding melt sagging [7]. Also,

* Corresponding author. Tel.: +49-421-218-5041; Fax: +49-421-218-5063.

doi:10.1016/j.phpro.2011.03.008

investigations on the influence of low-frequency alternating magnetic fields on melt bead dilution in laser beam welding of aluminium with Si-containing filler wire were performed. A homogeneous silicon distribution above 2% throughout the seam can significantly decrease the hot-crack susceptibility of aluminium alloy (e.g. 6XXX-alloys) [8]. This so-called magnetic "stirring" technique has been successfully applied to modify Si dilution [9]. A full review on the application of electromagnetic fields in arc and laser beam welding is given by Vollertsen and Thomy [10]. Yet, the effect of the alternating magnetic fields on the element distribution is predominantly known from experiments, especially metallographic inspections of the resulting weld seam [11]. To obtain a more profound knowledge about the stirring effect taking place inside the liquid melt pool, both experimental and theoretical research efforts have been taken recently to fully understand the complex, mainly fluid dynamic processes during laser welding in the presence of a magnetic field [12]. A more profound understanding of these interactions in dependence of the process parameters might promote the ability to significantly increase the homogeneity of the element distribution of filler material in the weld seam.

To access the problem theoretically, it is advisable to use a CFD model since both the fluid-dynamic phenomena induced by the laser irradiation and the interaction between the liquid melt pool and the magnetic field can be dealt with applying the Navier-Stokes-equation. Modelling the laser beam welding process [13] and laser beam hybrid welding [14] is part of several research activities around the globe. Depending on the primary aim of the respective numerical investigations, some of the welding phenomena are modelled in more detail (e.g. the laser beam absorption process [15] or effects of contamination (e.g. the influence of zinc coating) [16]) and some other are rather simplified to keep the required calculation time at an acceptable degree.

2. Aim and scope

The aim of the work presented here is to promote a deeper understanding of the influence of the magnetic stirring effect on the concentration distribution of filler wire material during full penetration laser beam welding of aluminium with a filler wire that contains an alloying element. The main focus of this work is the theoretical understanding of the complex and transient fluid dynamic interactions between the magnetic field and the laser induced liquid melt pool that leads to a specific concentration distribution of the filler material after solidification. A CFD model, involving the main driving forces of the process, is therefore presented. This model can be used to calculate a welding sequence of about 0.3 s within an adequate calculation time. The model was applied to investigate the influence of different frequencies and flux densities of the magnetic field on the resulting element distribution. For comparison, a full penetration laser welding experiment on Al99.5 aluminium was performed using a hyper eutectic filler wire with a very high silicon content of 18%.

3. Experimental setup and procedure

The welding experiments were carried out with a TruDisk8002 disc laser at an output power of 5.5 kW. Focal length of the optics (Trumpf optics) was 250 mm and collimation length was 250 mm. With a fiber diameter of 200 µm the nominal focal spot size was 200 µm. Full penetration bead-on-plate welding was performed on 3 mm thick Al99.5 sheets with the focal position 2 mm above the specimen. A prototype AlSi18 wire (with an average silicon content of 18% [17]) of diameter 1.2 mm was used as filler material. The welding velocity was v_0 = 8 m/min and the wire feeding rate was v_d = 6 m/min, respectively. With the chosen laser power and welding velocity, the experiment was performed as full penetration welding.

A magnetic field of different reference flux densities B_0 and different frequencies f was supplied by the welding head shown in Figure 1(a). The DC flux density distribution $\widehat{B}(B_0, r, z)$ of the magnetic field was coaxial to the laser beam with the amplitude of the flux density decreasing slightly with increasing axial distance from the welding head (see Figure 1(b)). The point of origin of this coordinate frame was set to the sheet surface and the laser axis. The time dependency or pulse shape of the magnetic field $b_{\sim}(t)$ shows a triangular shape as given in Figure 1(c). After welding, longitudinal sections of the specimen are taken and analyzed using EDX method to quantify the silicon distribution.

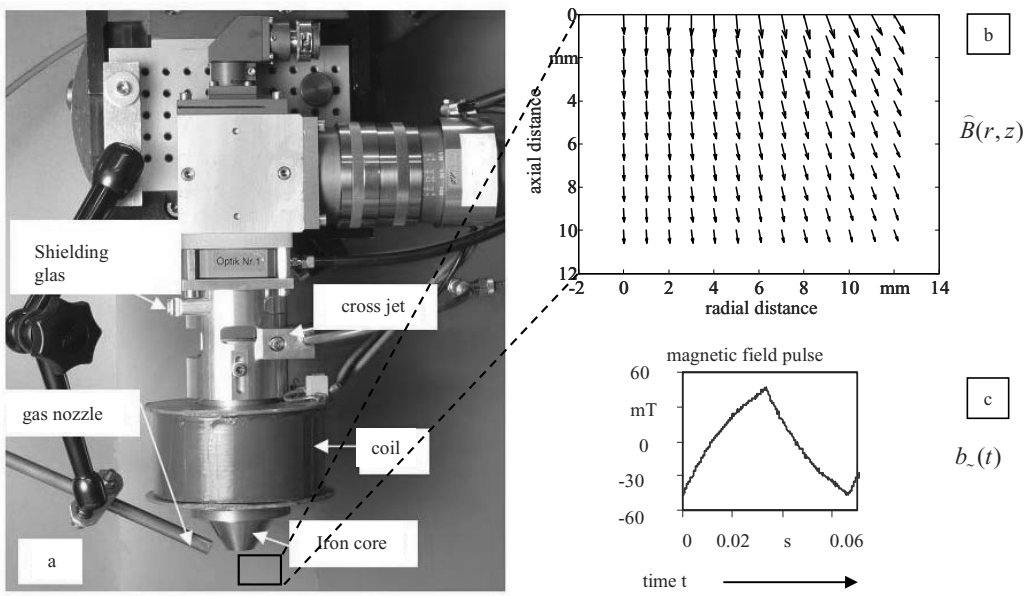

Figure 1. Welding head prototype to supply both laser beam and coaxial magnetic field (a), flux density distribution below the protruding iron core (b) and pulse shape of the magnetic field (c)

4. Development of the numerical model

A CFD model of full penetration bead-on-plate welding with additional filler wire has been developed to calculate the melt flow under influence of an alternating magnetic field which is aligned nearly coaxially to the laser beam (see Figure 1(b)). In order to calculate the melt pool and seam geometry together with the filler wire, a model geometry as shown in Figure 2 is used. It consists of a 3 mm thick quadrangular geometry of thickness 3 mm that forms the aluminium sheet. A cylindrical body of radius 0.6 mm is attached to this geometry to account for the filler wire. Both geometries are partially penetrated by a rotationally symmetric geometry that follows a typical keyhole shape. This simplified keyhole model (based on the work of [18]) enables the simulation of the laser beam absorption by attaching the evaporation temperature to the surface of the keyhole geometry.

To account for the main driving forces like the flow around the keyhole, Marangoni convection and buoyancy inside the melt pool along with phase change effects such as the evolution of latent heat or the solidification/melting specific model implementations are done predominantly by adding force and energy sources to the momentum and energy equation.

Buoyancy effects are considered by adding a volume force according to

$$f_{buoy} = \left(\rho - \rho_{ref}\right) \cdot \vec{g} \tag{1}$$

to the momentum equation in which $\vec{g}$ describes the gravitational acceleration, ρ the local density and ρ_{ref} the reference density of the fluid at the melting temperature, respectively. This formulation requires a temperature dependent density. To allow for the phase change, the latent heat evolution has to be considered. The enthalpy is therefore described as

$$h = c_p\left(T - T_0\right) + \beta \cdot \Delta H \tag{2}$$

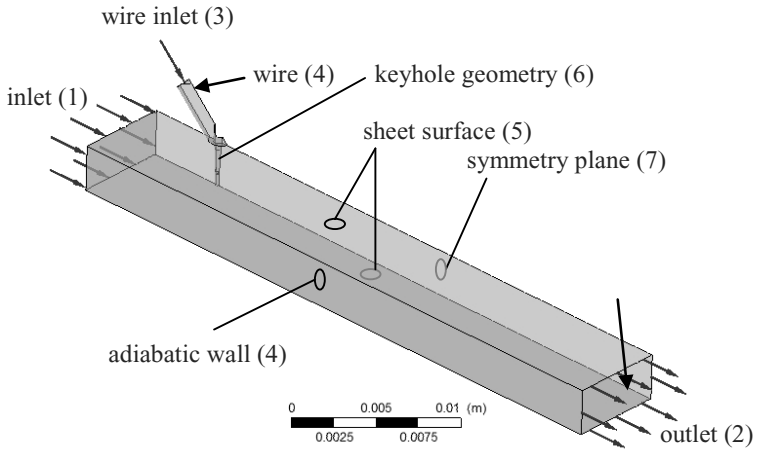

B-#	Momentum	Energy
1	$v_n = 0.133$ m s^{-1}	T = 300 K
2	hydrostatic pressure	$\frac{\partial T}{\partial \vec{n}} = 0$
3	$v_n = 0.1$ m s^{-1}	T = 300 K
4	$\frac{\partial \vec{v}}{\partial \vec{n}} = 0$	$\frac{\partial T}{\partial \vec{n}} = 0$
5	local specified shear stress	$\frac{\partial T}{\partial \vec{n}} = 0$
6	$\frac{\partial \vec{v}}{\partial \vec{n}} = 0$	T = 2700 K
7	symmetric	symmetric

$\vec{n}$ = boundary normal vector

Figure 2. Model geometry of the process with filler wire and approximated keyhole shape (left) and list of dynamic and thermal boundary conditions (right)

with c_p, T, T_0 and ΔH being the specific heat capacity at constant pressure, temperature of the control volume, ambient temperature and latent heat of fusion, respectively. β describes the so called liquid fraction that follows from

$$\beta = \min\left[1, \max\left[0, \frac{T - T_S}{T_l - T_S}\right]\right] \tag{3}$$

with T_S and T_L being the solidus and liquidus temperature, respectively. Within a temperature range of 34 K the liquid fraction of the control volume transfers from 0 to 1. To simulate the solidification dynamically, a volume force according to

$$f_{s/l} = C_0\left(\vec{v} - \vec{v}_0\right) \tag{4}$$

is added to the momentum equation to reduce any liquid movement to that of the solid metal which is moving with the welding velocity $\vec{v}_0$. $\vec{v}$ and C_0 are the velocity field and a force factor that defines the strength of the volume force, respectively. In comparison to another model implementation [11] in which free surfaces were considered, the calculations given herein are performed for a single phase model for simplicity. Hence, surface deformations are neglected and surface tension effects are introduced as boundary conditions. The Marangoni convection can be simulated by adding a boundary force according to

$$f_{Marangoni} = \gamma_T \cdot \nabla T \tag{5}$$

with ∇T being the local temperature gradient and γ_T the surface tension temperature coefficient. This results in an acceleration of the liquid along the temperature gradient. In case of a negative temperature coefficient (which is the case for the aluminium material used this model) the acceleration is aligned towards a decreasing temperature.

The interaction between the magnetic field and the conducting fluid with velocity field $\vec{v}$ induces a current density inside the moving melt and base material. Together with other external or internal electric fields $\vec{E}$ the current density is described by

$$\vec{j} = \sigma\left(\vec{E} + \vec{v} \times \vec{B}_{ext}\right) \tag{6}$$

with σ being the electrical conductivity and B_{ext} the flux density of the external AC magnetic field. The latter is the product of the local DC density distribution $\tilde{B}(B_0, r, z)$ shown in Figure 1(b) and the pulse shape $b_{\sim}(t)$ shown in Figure 1(c). An empirical description of $\tilde{B}(B_0, r, z)$ in dependence of the reference flux density B_0 is given elsewhere [11]. The pulse shape of the magnetic field is approximated by

$$b_{\sim} = 1 - \frac{2}{\pi}\arccos\left(\cos\left(t - t_0\right)\right) \tag{7}$$

which describes a triangular shape with t and t_0 being the time and time-offset, respectively. The interaction between the current density and the external field entails a volume (Lorentz) force according to

$$f_L = \vec{j} \times \vec{B}_{ext} \tag{8}$$

that is also added to the momentum equation.

The material properties of the fluid used in these calculations are those of pure aluminium (liquid and solid). They are listed in Table 1. They are assumed for the base material and the filler wire as well to simplify the calculation. The silicon that is supplied by the filler wire was included as an additional mass free scalar quantity ϕ, which temporal and spatial distribution was calculated by an additional transport equation

$$\frac{\partial \phi}{\partial t} + \nabla\left(\vec{v}\phi\right) = 0\,. \tag{9}$$

It is calculated based on the calculated velocity field. A value of $\phi = 1$ characterizes a 100% alloying element content in a control volume, while a value of $\phi = 0.18$ which was assumed at the wire inlet boundary, characterizes a content of 18% of the alloying element. Other alloying elements both of the base material and the filler wire are neglected. Diffusion effects are not yet considered in these model calculations.

The dynamic and thermal boundary conditions used for the calculations are listed in Figure 2. The governing equations are solved with the finite volume method using the commercial CFD-solver CFX5.1 with high resolution advection scheme [19] and a first order backward Euler scheme to calculate the flow transiently. The model geometry is therefore discretized into approximately 1 million tetrahedral control volumes. A steady state solution without taking the magnetic field into account is used as initial condition for the transient calculations. The time step assumed is 1e-03 s. Overall duration of the simulated welding process is 0.3 s starting from the quasi-static solution.

Table 1. Material properties used in the simulation [20, 21]

Material property	Liquid	Solid	Unit
Density	Temp. dep.	2385	kg m^{-3}
Spec. heat capacity	1080	Temp. dep.	J kg^{-1} K^{-1}
Thermal conductivity	Temp. dep.	Temp. dep.	W m^{-1} K^{-1}
Viscosity	0.0013	100	N s m^{-2}
Electrical conductivity	Temp. dep.	Temp. dep.	S m^{-1}
Latent heat of fusion	398	-	kJ kg^{-1}
Surface tens. temp. coef.	-0.115	0	mN m^{-1} K^{-1}
Solidus temperature T_S	-	899	K
Liquidus temperature T_L	933	-	K
Solidification constant C_0	0	$5*10^9$	N s m^{-4}

5. Results

5.1. Influence of the frequency

Calculations are performed for a welding velocity of v_0 = 8 m/min and a wire feed rate of v_d = 6 m/min. To investigate the influence of the frequency of the magnetic field on the element distribution ϕ, a fixed reference flux density of B_0 = 160 mT is chosen. The calculations are performed for a frequency of 10 Hz, 15 Hz and 20 Hz. In Figure 3 the concentration distribution of ϕ after 0.3 seconds of welding is shown along the longitudinal symmetry plane of the model system geometry as a coloured field plot. The black line indicates the melting isothermal line along the specimen and filler wire that surrounds the molten pool. The filler wire material is diluted through the melt pool according to the strong convections resulting from buoyancy effects, flow around the keyhole, Marangoni effect and the induced magnetic volume force. The melt pool is slightly elongated near the surfaces especially at the top surface.

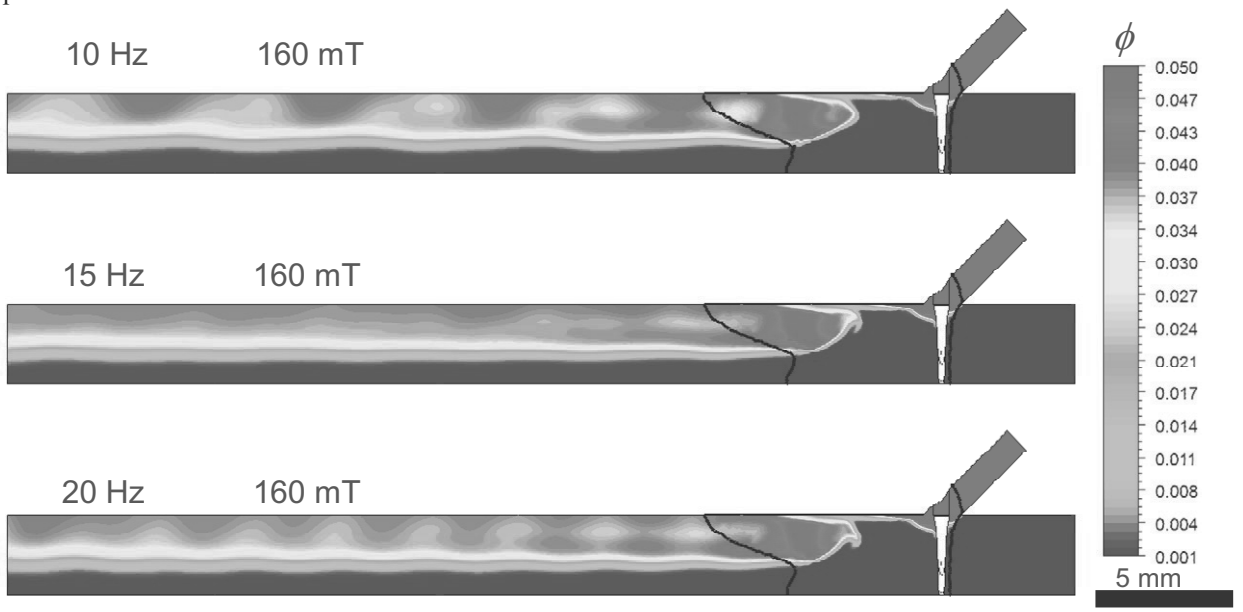

Figure 3. Distribution of the mass free quantity ϕ at the longitudinal section (colored plot) and melting isothermal line (black line).

In the solidified area left from the melt pool, the concentration of ϕ is spatially modulated. By trend, the highest concentration can be found near the top surface, whereas no filler material can be found near the bottom surface. At a frequency of 10 Hz and 20 Hz the spatial modulation is clearly periodically; areas of high concentration and lower concentration are locally patterned. Using a frequency of 15 Hz, the resulting concentration distribution has no significant modulation.

Additionally to this perspective, the resulting ϕ concentration is shown at the top surface of the model geometry in Figure 4. After solidification, the highest concentration of the filler material can be found near the symmetry plane which would be the middle of the weld seam. Similar to the distribution at the longitudinal section, the spatial modulation of the filler material is periodical for a frequency of 10 Hz and 20 Hz and shows no significant modulation for a frequency of 15 Hz.

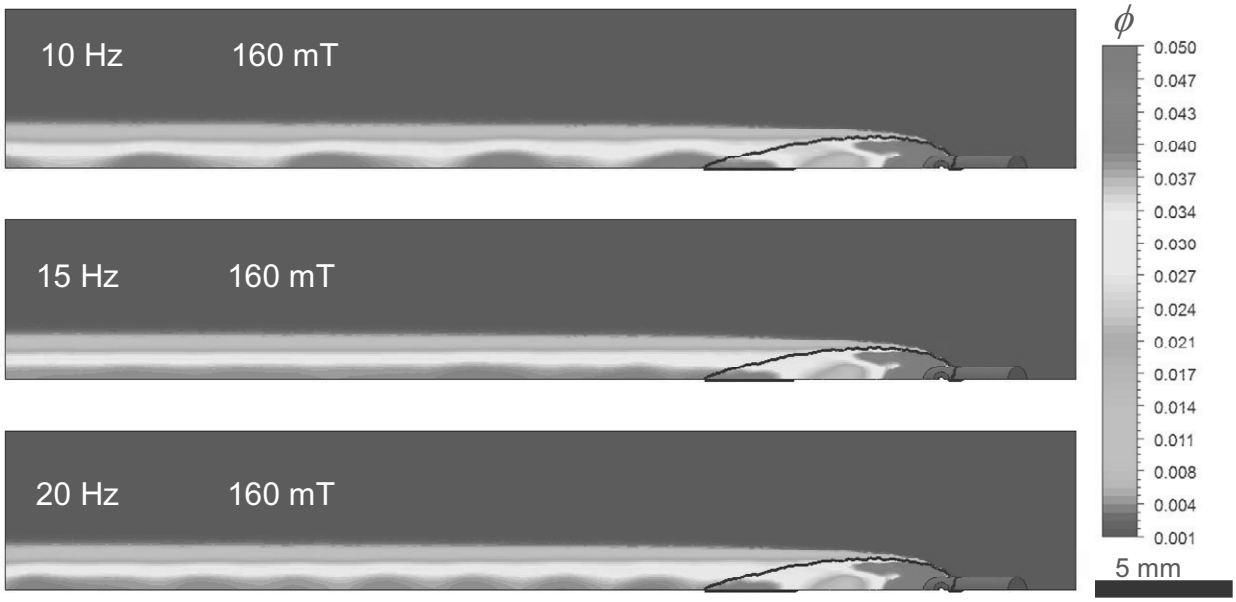

Figure 4. Distribution of the mass free quantity ϕ at the longitudinal section (colored plot) and melting isothermal line (black line).

5.2. Influence of the flux density

A second series of calculations is performed to investigate the influence of the reference flux density B_0 on the element distribution. In this case the frequency is fixed to a value of 10 Hz whereas the reference flux density is set to 160 mT, 260 mT and 360 mT, respectively. The calculated concentration distribution of ϕ at the longitudinal symmetry plane is shown in Figure 5.

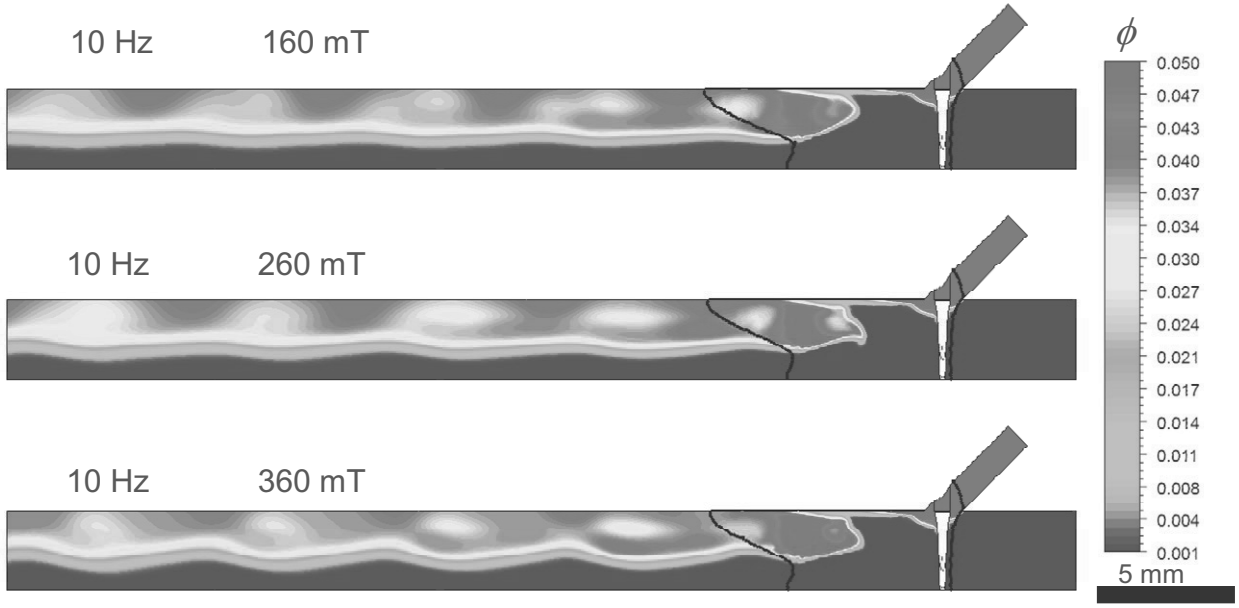

Figure 5. Distribution of the mass free quantity ϕ at the longitudinal section (colored plot) and melting isothermal line (black line).

The periodic pattern of the concentration distribution is changing its shape with increasing flux density. A slight tendency towards a more homogeneous concentration in the upper half of the weld seam for an increasing flux density can be noticed.

In Figure 6 the distribution for increasing flux density is shown at the top surface. The flux density shift from 160 mT to 260 mT from this perspective seems to have little effect on the distribution, whereas a slight narrowing of the patterns with high concentration can be noticed at a value of 360 mT.

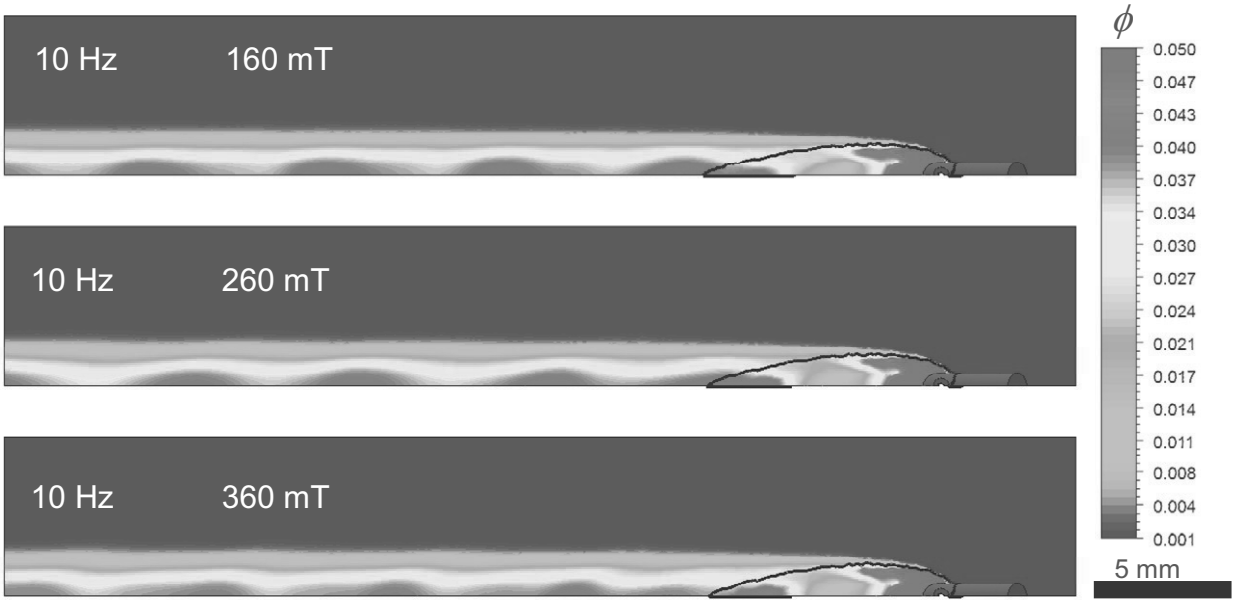

Figure 6. Distribution of the mass free quantity ϕ at the sheet surface (colored plot) and melting isothermal line (black line) for different flux densities at a fixed frequency of 10 Hz.

5.3. Experimental Results

For comparison, the silicon distribution of welded specimens (see chapter 3) is quantified by EDX-scans of their longitudinal section. A result is shown in Figure 7. The white areas are indicating high silicon concentration while the dark areas are predominately consisting of base material.

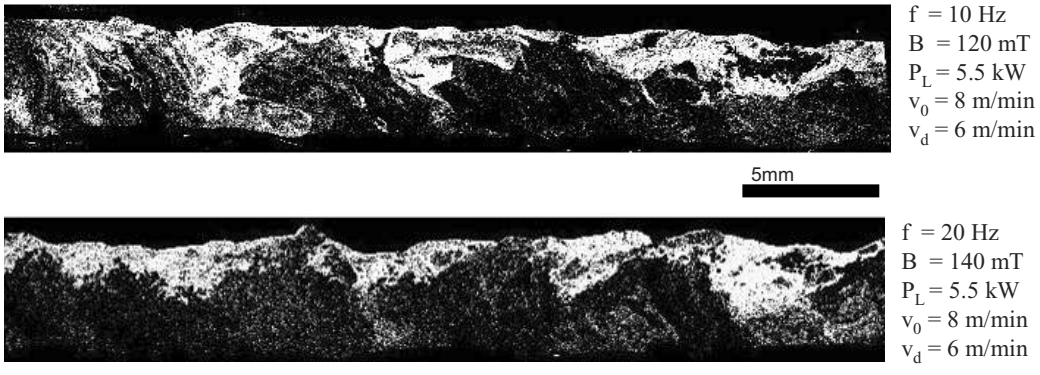

Figure 7. Distribution of silicon measured with EDX method at the longitudinal section (bright areas indicating high silicon content) for different fields.

Comparable to the calculated quantity ϕ, the silicon concentration distribution also shows a periodical pattering of high and low concentration areas, though the frequency of the concentration alternation differs slightly from the calculation results. The highest concentrations can be found near the top surface of the weld seam, whereas the maximum depth of the high concentration patterns is slightly higher than half of the overall weld seam depth.

6. Discussion

From recent research it is known that the induced Lorentz forces can have a significant impact on the velocity field inside the molten pool. The forces are mainly acting against the original melt flow if the fluid is flowing at an angle to the magnetic field [22]. Otherwise, no electric current is induced and hence no volume forces occur. The main flow direction in the melt pool is from the keyhole front to the melt pool rear, nearly perpendicular to the magnetic field.

Under this assumption, a suitable explanation of the calculated concentration distribution, especially the periodical pattern, would be a periodically modulation of the velocity field inside the melt pool causing a deflection of the melt flow. The Lorentz forces should mainly act in the horizontal direction as can be easily understood from the vector relation in equation (6) and (8), which is then causing the flow resistance. The reaction of the melt flow is a deflection in a horizontal direction to decrease the angle between the magnetic field and the melt flow in order to reduce the flow resistance. The modulated melt flow is then mainly determining the element distribution, besides secondary effects, like the diffusion, which is however neglected in the simulations presented here.

Since the magnitude of the volume forces is proportional to the local velocity, the highest forces are induced in the region of high velocities. From the calculation results, the highest velocities can be found near the upper and lower surface due to the Marangoni acceleration. Beside this, the slight inhomogeneity of the magnetic field both in radial and axial direction has to be considered. The highest flux density values are near the upper surface of the melt pool. Hence, taking into account the strong acceleration due to the Marangoni convection, the induced forces should be highest in this region. This assumption is also in agreement with other results [12].

A second effect that has to be considered is the deflection of the melt flow at the rear melt pool boundary that also causes a flow from the surfaces to the interior of the melt pool (even without any magnetic fields). This flow pattern is also modulated by the induced forces and should affect the resulting concentration distribution.

The calculations on the influence of the frequency have revealed a periodic modulation of the concentration distribution (especially for 10 Hz and 20 Hz). That could be understood easily due to the pulsing force induced by the magnetic field together with the deflection of the melt flow. It is important to notice that the modulation is not always strictly periodic. With 15 Hz no significant modulation is visible. This might be explained by a general transient instability of the melt flow, also without any additional magnetic field. The resulting distribution at 15 Hz could then be a superposition of transient effects from the general flow instability together with the flow modulation due to the magnetic field and could cause some interference that hinders a periodic pattering.

The periodic pattering of the concentration can be confirmed from the experimental results. Only the frequency of the pattering is different to that of the calculation results. That could be caused by simplifications in the model, especially of effects induced by instabilities of the keyhole.

The flux density seems to have a significant impact on the homogeneity of the element distribution. It can be seen from the calculations that with increasing flux density the patterns of high and low concentrations are more blurred, which indicates that the homogeneity of the concentration is slightly increased.

7. Conclusion

The influence of an external applied inhomogeneous coaxial magnetic field on element distribution of filler wire material in the weld seam during laser beam welding was investigated using a numerical model. It was established that both the frequency of the magnetic field and the flux density have an effect on the resulting filler wire material distribution and the concentration of alloying elements in the remaining weld seam. The frequency is mainly determining the patterning of local concentration resulting in both a periodical patterning and a concentration distribution without a specific modulation as well. The flux density defines the absolute value of the induced volume forces and seems to have an effect on the homogeneity of the concentration distribution, as well.

Acknowledgements

This work was accomplished within the Center of Competence for Welding of Aluminum Alloys - Centr-Al. Funding by the DFG (Vo 530/29-2) is gratefully acknowledged.

References

[1] Asai, S.; Nishio, N.; Muchi, I.: Theoretical Analysis and Model Experiments on Electromagnetic Driven Flow in Continuous Casting. In: Transactions of the Iron and Steel Institute of Japan Vol. 22, No. 2 (1982), 126-133.
[2] Mousavi, M.G.; Hermans, M.J.M.; Richardson, I.M. u.a.: Grain refinement due to grain detachment in electromagnetic stirring of AA7020 welds. In: Science and Technology of Welding and Joining 8 (2003), 4, 309-312.
[3] Moreau, R.: Magnetohydrodynamics. Kluwer Academic Publishers, Dordrecht, 1990.
[4] Ambrosy, G.: Nutzung elektromagnetischer Volumenkräfte beim Laserstrahlschweißen. Dissertation, Herbert Utz Verlag, München, 2009.
[5] Tang, Z.; Gatzen, M.; Vollertsen, F.: Experimental investigation of the melt flow in Aluminum during laser welding with magnetic stirring, In: Proc. of Pacific International Conference on Applications of Lasers & Optics (PICALO'10), (2010), paper 403 (CD-Rom).
[6] Lindenau, D.; Ambrosy, G.; Berger, P. u.a.: Magnetisch beeinflusstes Laserstrahlschweißen. In: Proc. Stuttgarter Lasertage SLT' 99, Stuttgart 1999, 39-56.
[7] Avilov, V.V.; Moldovan, R.; Berger, P.; Graf, T.: Electromagnetic weld pool control systems for laser beam welding of thick metal plates, In: Proc. of IWOTE'08 International Workshop on Thermal Forming and Welding Distortion, Bremen, April 22 – 23, (2008), 413 – 420.
[8] Kou, S.: Welding Metallurgy, 2nd ed. Hoboken, Wiley-Interscience, John Wiley&Sons, New Jersey, 2003.
[9] Thomy, C.; Vollertsen, F.: Application of Alternating Magnetic Fields in Laser Welding of Aluminium. In: Proc. Of LAMP2006, 4th International Congress on Laser Advanced Materials Processing, Kyoto, Japan, 2006.
[10] Vollertsen, F.; Thomy, C.: Magnetic Stirring during Laser welding of Aluminium. In: Journal of Laser App. 18 (2004), 28 – 34.
[11] Tang, Z.; Gatzen, M.: Influence on the dilution by laser welding of aluminium with magnetic stirring. In: Laser Assisted Net Shape Engineering (LANE2010) Physics Procedia 5/2, eds.: M. Schmidt, F. Vollertsen, M. Geiger. Meisenbach Bamberg (2010), 125 – 137.
[12] Gatzen, M.; Tang, Z.: CFD-based model for melt flow in laser beam welding of aluminium with coaxial magnetic field. In: Laser Assisted Net Shape Engineering (LANE2010), Physics Procedia 5/2, eds.: M. Schmidt, F. Vollertsen, M. Geiger. Meisenbach Bamberg (2010), 317 – 326.
[13] Geiger, M.; Leitz, K.-H.; Koch, H.; Otto, A.: A 3D transient model of keyhole and melt pool dynamics in laser welding applied to the joining of zinc coated sheets. In: Prod. Eng. Res. Devel. 3, No. 2, (2009), pp. 127 – 136.
[14] Na, S.-J.; Cho, J. H.: Three-Dim. Analysis of Molten Pool GMA-Laser Hybrid Welding. In: Welding Journal 88(1), (2009), 35 – 43.
[15] Koch, H.; Leitz, K.-H.; Otto, A.; Schmidt, M.: Laser deep penetration welding simulation based on a wavelength dependent absorption model, In: Physics Procedia, Volume 5, Part 2, (2010), 309-315.
[16] Schmidt, M.; Otto, A.; Kägeler, C.: Analysis of YAG laser lap-welding of zinc coated steel sheets, In: CIRP Annals – Manufacturing Technology 57, (2008), 213 – 216.
[17] Buschenhenke, F.; Seefeld, T.; Vollertsen, F.: Laser welding of high strength aluminium sheet with hypereutectic AlSi filler wire, In: Proc. of International Conference on Applied Production Technology (APT'07), eds.: F. Vollertsen, C. Thomy. BIAS-Verlag, Bremen (2007), 135 – 145.
[18] Jüptner, W.; Rothe, R.: GFA-BASIC-Programm zur Berechnung des Dampfkanals beim Laserstrahlschweißen. BIAS Verlag Bremen (1986).
[19] N. N.: Handbook, Manual ANSYS CFX 12.0, ANSYS Corp., Berlin, 2009.
[20] Brandes, E. A.; Brook, G. B.: Smithells Metals Reference Book, Butterworth-Heinemann, Oxford, Boston, 1998.
[21] Kalazhokov K.K.; Kalazhokov, Z.K.; Khokonov, K.B.: Surface tension of pure aluminium melts. In: Technical physics, vol. 48, No 2, pp. 272-273, 2003.
[22] Gatzen, M.; Tang, Z.; Vollertsen, F.: Influence of a magnetic field in laser beam welding of aluminium. In: Proc. LAMP 2009 in Kobe/Japan, online-proceedings (http://www.jlps.gr.jp/en/proc/lamp/09/), #09-137 (#170).